

You Zhou
Jicheng Shen
Weihua Wei ✉
Fang Luo

<https://doi.org/10.21278/TOF.492069024>
ISSN 1333-1124
eISSN 1849-1391

OPTIMIZATION OF THE TRANSMISSION TUBE OF A BALL MILL BASED ON THE EDEM-WORKBENCH METHOD

Summary

The structural design of the transmission tube significantly influences its mechanical behaviour under operating conditions, making structural optimization crucial for improving the performance and reliability of a ball mill. In this paper, the response surface method and multi-objective genetic algorithm are used to carry out optimization research on the existing BM4213 ball mill transmission tube structure to address the problem of its large size and size-related material costs. Firstly, the discrete element simulation of a transmission tube based on the Altair EDEM software is carried out to analyse the movement of the material in the transmission tube and determine the load acting on it. Thereafter, the load exerted on the transmission tube by the material is imported into the static analysis module in Workbench to obtain the stress and deformation of the transmission tube at full load start-up using the coupled EDEM-Workbench method. Subsequently, the part of the design to be optimized is determined based on the results of the static analysis. Finally, a mathematical model of the transmission tube optimization design is constructed; using the response surface optimization module in Workbench and a multi-objective genetic algorithm, a comprehensive optimization design of the transmission tube is carried out. The structural dimensions in the mathematical model of the transmission tube are adjusted to effectively reduce its stress and mass. The optimized transmission tube exhibited reductions of 6.735% in mass, 9.188% in maximum stress, and 16.721% in maximum deformation. This research provides an essential reference for the optimized design of the BM4213 ball mill transmission tube.

Key words: Ball mill, EDEM-Workbench method, Static analysis, Response surface method, Optimized design

1. Introduction

Ball mills have been widely used in cement, metallurgy, mining, construction, and other industries due to their advantages of large crushing ratio, simple structure, strong material adaptability, and easy handling [1–3]. The main components of a ball mill are the feeding device, the rotary body, and the transmission device. The rotary body structure is mainly composed of a transmission tube and a barrel, as shown in Fig. 1. The transmission tube is one of the key components of the ball mill rotary body; it connects the ball mill barrel to the

transmission device. The transmission tube has the following main functions: (1) rotate the barrel of the centre-drive ball mill through the transmission device; (2) discharge the material that has been ground in the ball mill barrel.

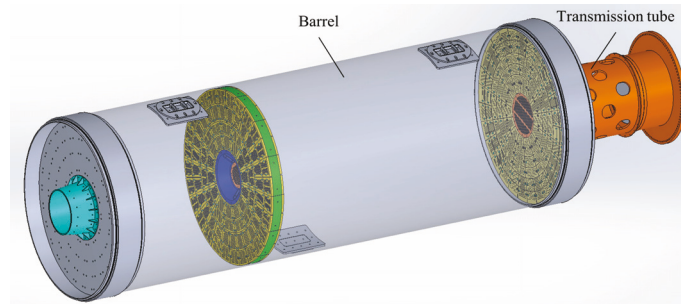


Fig. 1 Structure of the rotary body

When the ball mill is running, the transmission tube is under a variety of loads, such as bending, shearing, and twisting, which will cause wear, tear, and fracture because of the impact of the materials after a long-term continuous operation [4–6]. Previous studies on the transmission tube are scarce, and some of them use the finite element method to check whether the stress and deformation of the transmission tube meet the design requirements [7]. Few of these studies investigate the movement of the material in the transmission tube. The research focuses on basic finite element analysis with insufficient attention paid to the material motion patterns and wear mechanisms [8]. In the structural design of the transmission tube, advanced algorithms are rarely used to optimize its design [9]. Some scholars ignore the influence of discrete materials in the strength analysis of the transmission tube to improve the calculation efficiency, which does not fully comply with the actual operation of the transmission tube [10,11]. Additionally, few current studies consider the coupling effect of structural parameters and operational performance, lacking a comprehensive multi-objective optimization approach and failing to adequately address the issue of weight reduction and structural integrity [12,13]. To address these limitations, we use the response surface methodology to optimize the structure while considering multiple performance objectives and manufacturing constraints, thus achieving significant improvements in the performance and reliability of the ball mill.

Co-simulation can fully utilize the advantages of multiple numerical analysis software to effectively solve complex engineering problems and significantly improve the simulation efficiency [14,15]. Engineering-Discrete Element Method (EDEM) is a mathematical analysis tool that relies on Newton's Second Law, as well as the Hertz and Mindlin-Deresiewicz theories of spherical particle contacts. EDEM is mainly used to analyse the processes of flow, accumulation, crushing, and extrusion of particle materials [16]. It provides a rich set of visualization and analysis tools that enable users to easily create parametric models of particle solids and simulate and analyse the loads applied to machine parts. The analysis results can be directly exported to the structural analysis tool of the user's selection, which greatly facilitates the user's research and design optimization [17,18]. In this paper, we study the movement of the material inside the transmission tube based on EDEM, and we obtain the load exerted on its inner wall by the material. Thereafter, the load data from EDEM is inputted into Workbench to perform a static analysis of the transmission tube. Finally, the response surface method and multi-objective genetic algorithm are used to optimize the transmission tube, and the optimization effect is analysed and evaluated in detail from the perspectives of stress and deformation to ensure that the optimal design effect is achieved. Figure 2 shows the flowchart of the overall framework for optimizing the structure of the transmission tube.

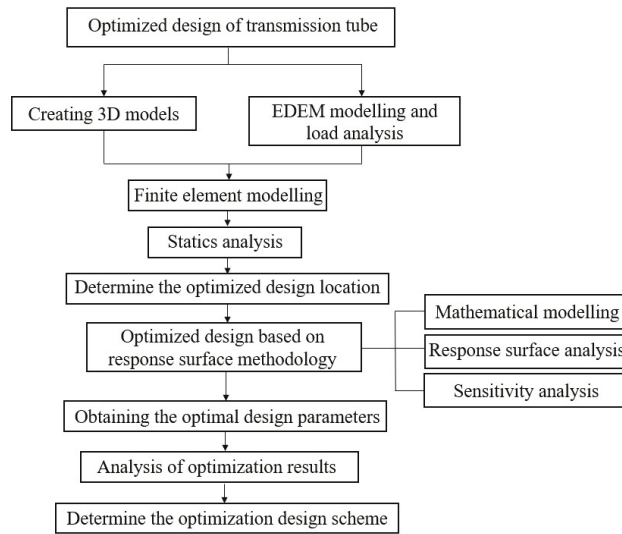


Fig. 2 Flowchart for optimized design

2. EDEM modelling and load analysis of the transmission tube

2.1 EDEM modelling

The discharge port and the blocking plate, two key components of the transmission tube, are retained in order to maintain their functionality when constructing a simplified model of the transmission tube. The bolt holes on the transmission tube are ignored to reduce the computational amount of finite element analysis and improve the computational efficiency [19]. SolidWorks is used to develop a 3D model of the transmission tube, as shown in Fig. 3.

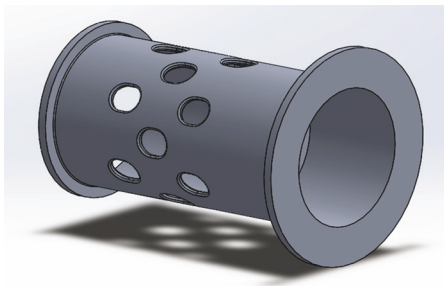


Fig. 3 3D model of the transmission tube

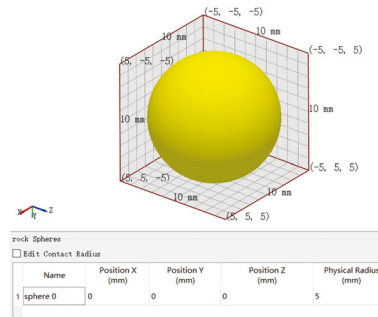


Fig. 4 Particle size setting

The particle radius should be chosen to be as small as possible in order to simulate the movement of the material more realistically. However, too small particles can lead to increased computational complexity and reduced computational efficiency [20,21]. After a comprehensive analysis, the particle radius size is set to 5mm, as shown in Fig. 4. That can improve the calculation efficiency and better simulate the movement of the material while ensuring the calculation accuracy.

Hertz–Mindlin (no slip) and Standard Rolling Friction are selected for the particle-to-particle contact model. The Hertz–Mindlin (no slip), Standard Rolling Friction, and Archard Wear models are selected for the model of the contact between the particles and the transmission tube to study the wear caused by the particles [22]. The wear constant in Archard Wear is set to 1×10^{-12} Pa [23], the transmission tube material is E235C, and the medium is ore. The specific parameters of material properties are shown in Table 1.

Table 1 Physical parameters of the model

Parameters	Transmission tube	Medium
Density	7864 kg/m ³	3135 kg/m ³
Poisson ratio	0.33	0.25
Static friction coefficient	0.5	0.5
Rolling factor	0.01	0.01
Recovery factor	0.5	0.5
Shear modulus	1×10 ¹⁰ Pa	1×10 ⁸ Pa

After grinding in the barrel, the material is discharged from the ball mill through the discharge port on the transmission tube [24]. A virtual particle plant with a diameter of 1700 mm and a thickness of 10 mm is set up at the inlet of the transmission tube to simulate the movement of the material. The output of this ball mill is 160 t/h (Fig. 5). Accordingly, the discharge speed is set to 45 kg/s, and the particles are generated from 0 s. The speed of the ball mill during the normal operation is 15.6 r/min. Consequently, the speed of the transmission tube is set to 1.5 rad/s, and the rotation starts from 0 s. The simulation time is set to 20 s. After completing the above-mentioned settings, EDEM can simulate the material entering the transmission tube at a speed of 45 kg/s, and the transmission tube rotates at 1.5 rad/s.

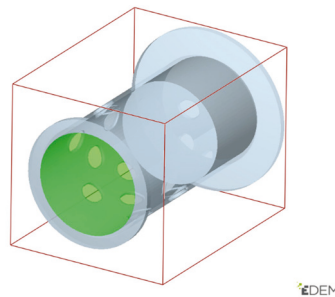


Fig. 5 Material particles

2.2 EDEM-based analysis of particle velocity in the transmission tube

In the analysis option of EDEM, we set the display of the particles to colour by velocity and generate the resultant velocity of the particles after the run is stable. The resultant velocity of the particles in the transmission tube is shown in Fig. 6. Figure 6(a) shows that the maximum velocity reaches 2.95 m/s when the particles approach the inner surface of the transmission tube. This portion of the particles has a high velocity. At the moment of contact with the transmission tube, this portion will exert an impact on the inner surface of the transmission tube and cause abrasion. The particles will accumulate in the tube after reaching the transmission tube and make a centrifugal motion with the transmission tube, as shown in Fig. 6(a) and Fig. 6(b) in the selected box No. 1. When this portion of the particles moves to the bottom of the discharge port, it is thrown out of the transmission tube with a velocity perpendicular to the inner surface of the transmission tube under the effect of centrifugal stress, as shown in the selected box No. 2 in Fig. 6(c). The selected box No. 3 in Fig. 6(c) shows that when the particles pass the edge of the discharge port, the velocity of the particles is perpendicular to the contact surface. At that moment, the particles will impact the discharge port due to the change in the velocity direction.

Figure 6(a) shows that the leftmost discharge port discharges most of the particles. The number of discharged particles decreases in order from left to right, and a small number of particles move near the blocking plate. The flowability of the particles near the blocking plate is poor. Consequently, the discharge efficiency of the transmission tube can be improved by properly adjusting the position of the blocking plate.

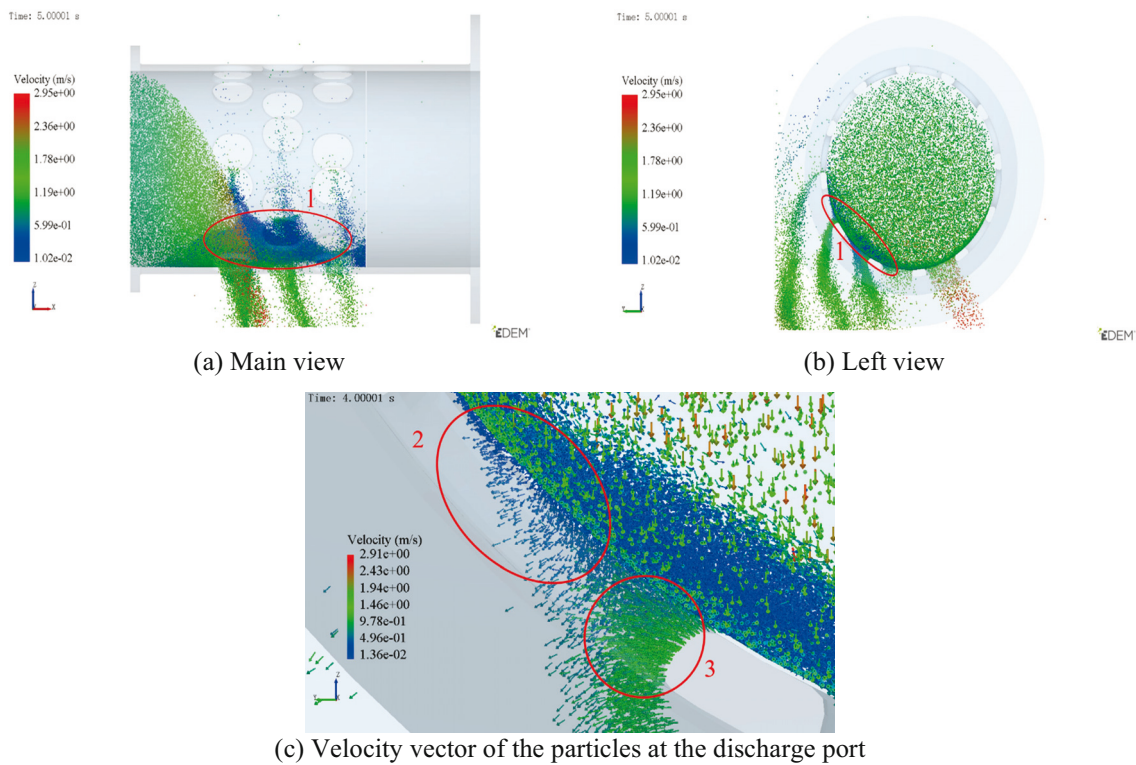


Fig. 6 Velocity of the particle motion

2.3 EDEM-based transmission tube wear analysis

Figure 7 shows the transmission tube wear distribution after 20 s of operation. The wear is mainly concentrated on the inner surface of the transmission tube and near the discharge port. According to Fig. 6(c), the velocity of the particles at the discharge port of the transmission tube rapidly changes. The wear depth produced by the particles on the discharge port after 20 s of operation is 1.27×10^{-6} mm. Majority of the particles are concentrated on the inner surface of the transmission tube after they enter the transmission tube and make a throwing motion. The maximum wear depth caused by the particles on the inner surface of the transmission tube is 5.07×10^{-7} mm after 20 s of operation. The comparison shows that the wear depth of the particles on the discharge port is greater than on the inner surface of the transmission tube.

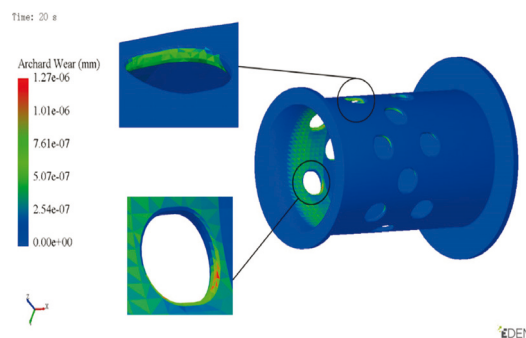


Fig. 7 Wear distribution on the transmission tube

2.4 EDEM-based transmission tube load analysis

Figure 8 shows the curve of the material load on the transmission tube as a function of time. The graph shows that the load on the transmission tube does not change in the period from 0 s to 0.5 s. Given that the particles have just started to enter at this time and have not

yet fallen on the inner surface of the transmission tube, the load is zero. The load on the transmission tube rapidly increases within the 0.5-1.5 s period due to the continuous falling of particles on the inner surface. In the 1.5-4 s period, the load on the transmission tube is reduced because some particles are discharged through the discharge port. The particle discharge speed and the entry speed reach balance within the 4-20 s period, and the transmission tube is in a relatively stable operating condition. At this time, the load on the transmission tube decreases and increases within a certain range.

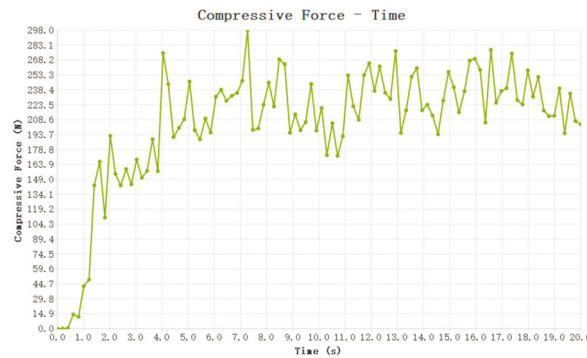


Fig. 8 Variation in the stress exerted on the transmission tube

The load on the transmission tube stabilizes after 4 s, and the maximum load is 298 N at 7.27 s. The minimal load of 173.196 N is applied at 10.3 s, and the average load is 235.347 N. In Figure 7, the load on the transmission tube at 6.87 s is close to 235 N. Therefore, the load applied at that moment is coupled with the static analysis module in the Workbench to perform a static analysis of it.

3. Static analysis of the transmission tube based on the EDEM-Workbench method

3.1 EDEM-based transmission tube load analysis

A simplified model of the transmission tube is imported into ANSYS Workbench. Automatic mesh division is applied to the transmission tube. Meanwhile, the grid encryption is applied to the discharge port. The maximum equivalent stress on the transmission tube is analysed for grid numbers 186481, 256370, 307858, and 347623. The result showed that the relative error is 1.1% at the grid number of 307858, and the maximum equivalent stress on the transmission tube is slightly affected by the grid. Therefore, the meshing of the transmission tube is carried out with the number of meshes at 307858, as shown in Fig. 9.

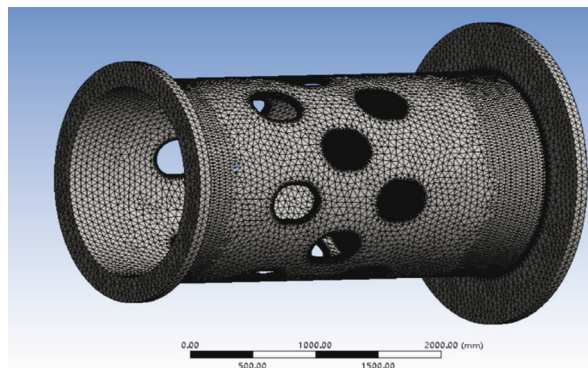


Fig. 9 Meshing of the transmission tube

The starting torque ($T=3.42 \times 10^6 \text{ N}\cdot\text{m}$) is loaded onto the right end of the transmission tube by applying a load to it in the static structural module of the ANSYS Workbench software. The output load data is imported into Workbench via EDEM in Workbench. The degrees of freedom (DOF) in each direction of the transmission tube must be limited

according to the actual operating conditions. The left end of the tube is constrained in a fixed manner, indicating that the displacement and rotation DOFs in three directions are constrained. The boundary conditions are set, as shown in Fig. 10. A cylindrical support is used to constrain the right end, limiting its axial and radial movements and releasing the rotational DOF.

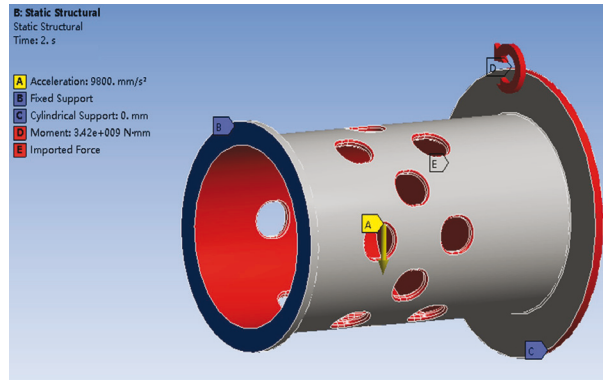


Fig. 10 Boundary conditions of the transmission tube

Two analysis steps are defined in the analysis setup, each with a step length of 1 s, to individually monitor the stress and deformation of the material on the transmission tube. The gravitational acceleration and starting torque are suppressed in the first analysis step to release the material stress on the transmission tube. The full load is released in the second analysis step.

3.2 Analysis of the results based on the EDEM-Workbench method

Figure 11(a) shows the equivalent stress of the transmission tube. Under the influence of material gravity, drive receiver self-weight, and starting torque, the maximum equivalent stress on the transmission tube occurs at the transition rounding on the discharge port, with a maximum value of 60.84 MPa. The stress values at both ends of the transmission tube are small. The equivalent stresses at all locations are less than 47 MPa, except at the transition rounding on the discharge port. The material of the transmission tube in this study is E235C. The yield limit of the material is 235 MPa, the maximum equivalent stress is 60.84 MPa, and the minimum safety factor is 3.86, which is much larger than the general safety factor of 1.5–2 required by the ball mill [25]. This result indicates that an optimal design may be achieved.

Figure 11(b) shows the deformation of the transmission tube. The deformation decreases from right to left. The maximum deformation occurs at its right end with a deformation of 0.927 mm. The minimum deformation occurs at its left end with a deformation of 0 mm. A targeted solution should be used to optimize the design of the structure in order to further improve its performance.

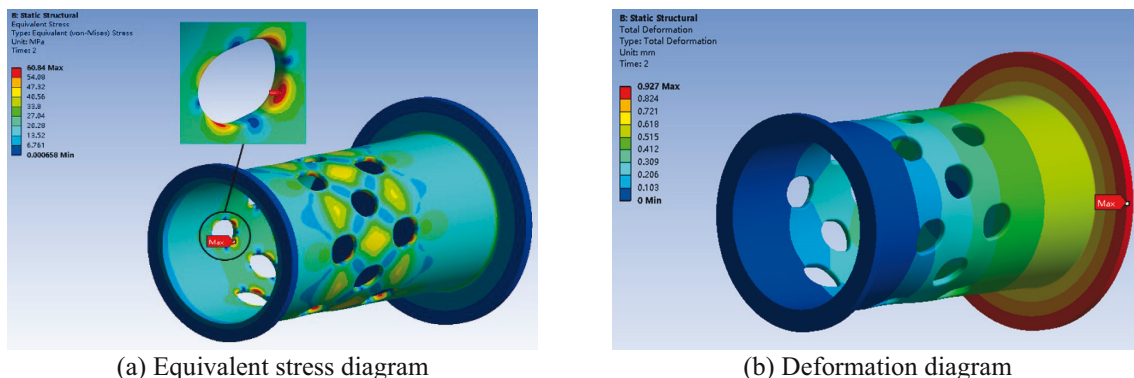


Fig. 11 Finite element analysis of the transmission tube

4. Optimization of the transmission tube based on the response surface method

Response surface method (RSM) is a statistical technique that creates mathematical models to describe the relationships between multiple design variables and response parameters through systematic sampling of the design space [26]. This method generates continuous response surfaces that can predict the system behaviour across the entire design domain. RSM can efficiently handle complex nonlinear relationships between geometric parameters and multiple objectives (mass, stress, and deformation) for the transmission tube optimization; it provides clear visualization of parameter interactions with less analysis than traditional optimization methods.

4.1 Analysis of the results based on the EDEM-Workbench method

The above static analysis shows that the stress on the transmission tube is concentrated at the transition corner on the discharge port, and the maximum stress value is much lower than the allowable value of the material. The stress values at both ends are small. Accordingly, an optimal design may be achieved. To improve the stability of cement ball mill operation and save manufacturing costs, in this section, the response surface method is adopted to optimize the structural design of the transmission tube.

In Fig. 12, the stresses on the transmission tube are mainly concentrated in the middle of the structure. The structural dimensions of the middle section can be defined by choosing x_1 and x_2 without changing its inner diameter (x_1 —thickness of the middle structure of the transmission tube; x_2 —length of the middle structure of the transmission tube). The design variables are taken in the following ranges: $65 \text{ mm} \leq x_1 \leq 75 \text{ mm}$ and $3100 \text{ mm} \leq x_2 \leq 3700 \text{ mm}$. The design variables are expressed in a matrix form as $x = (x_1, x_2)^T$.

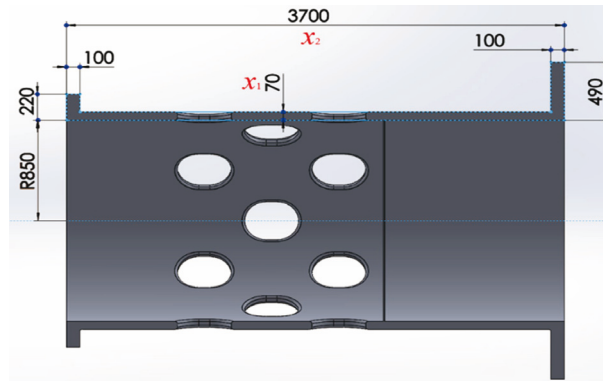


Fig. 12 Definition of the variable parameters

A 5% reduction in the mass of the transmission tube is set as the optimization target to achieve a more significant optimization effect: $g_2(x) = m_{\max} - [m_s] \leq 0$. ($m_s = M \times 5\% = 12540 \text{ kg}$).

The transmission tube, which is a key component of the ball mill, transmits torque and has a role in the discharging of the material. Therefore, the structure of the transmission tube must be optimized to reduce the stress value and improve the stability of the ball mill during the operation. The stress minimization of the transmission tube is set as the optimization objective. The design objectives are expressed in the following formula: $f_\sigma(x) = \sigma(x) = \sigma(x_1, x_2)$. In summary, the mathematical model of this response surface optimization design is as follows:

$$\begin{cases} x = (x_1, x_2)^T \\ g_2(x) = m_{\max} - [m_s] \leq 0 \\ f_\sigma(x) = \sigma(x) = \sigma(x_1, x_2) \end{cases} \quad (1)$$

4.2 Response surface method employed in the optimization design process

Response surface optimization of transmission tube consists of three main parts: geometry module, static analysis module, and optimization module. As shown in Fig. 13, the optimization design process provides an efficient and accurate optimized design of the transmission tube. In the geometry module, a simplified model of the transmission tube is established, and the design variables are defined as input parameters. Through the EDEM in Workbench, the loads obtained in EDEM are coupled into Workbench. After the solution is completed, the mass, maximum equivalent force, and maximum deformation of the transmission tube are set as the output parameters, and the corresponding input and output parameter sets are established. After these parameter sets are imported into the optimization module, the design of experiments, response surface fitting, and optimization solving will be carried out sequentially [27]. Finally, after the optimization solution has been reached, the optimal parameter combination of the transmission tube will be obtained.

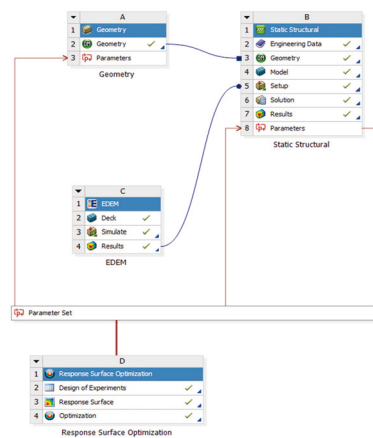


Fig. 13 Response surface optimization design process

4.2.1 Experimental design based on central composite design

Central Composite Design (CCD) combines factorial and axial points for efficient response surface estimation [28]. In the transmission tube optimization, CCD effectively manages multiple parameters and nonlinear relationships while reducing computational cost through orthogonal design. These advantages make CCD ideal for balancing performance objectives within manufacturing constraints. Response surface optimization requires a Design of Experiments for the transmission tube, which generates multiple sets of experimental design points based on the range of design variables [29]. In Table 2, nine sets of representative experimental design points are generated using the CCD method based on multiple pretests. Design point 1 (P1) corresponds to x_1 , P2 corresponds to x_2 , P4 corresponds to the mass of the transmission tube, P5 corresponds to the maximum equivalent stress, and P6 corresponds to the maximum deformation.

Table 2 Nine groups of experimental design points

Serial number	P1 (mm)	P2 (mm)	P4 (kg)	P5 (MPa)	P6 (mm)
1	70	3400	12587.52	60.70993	0.889624
2	65	3400	11937.47	67.05997	0.968203
3	75	3400	13241.54	55.36522	0.822140
4	70	3100	11669.20	60.56853	0.833091
5	70	3700	13505.82	61.01291	0.946178
6	65	3100	11087.14	66.91012	0.906794
7	75	3100	12254.84	55.34393	0.769826
8	65	3700	12787.76	67.19563	1.029628
9	75	3700	14228.21	55.57189	0.874475

4.2.2 Sensitivity analysis

Sensitivity analysis visualizes the effect of each design variable on the output variables and provides a reference for the optimal design of the transmission tube [30]. The sensitivity analysis of design variables P1 and P2 on P4, P5, and P6 is shown in Fig. 14. The sensitivity of P1 and P2 to P4 is positively correlated. This finding indicates that the mass of the transmission tube increases with the increase in the values of P1 and P2, where the degree of influence of P2 on the mass is greater than that of P1. Design variables P1 and P2 have positive and negative sensitivities to P5. The design variable P1 has a greater effect on the maximum equivalent stress on the transmission tube and is negatively correlated. This notion indicates that the value of the maximum equivalent stress on the transmission tube decreases with the increase in the value of P1. The sensitivity of P2 to the maximum equivalent stress in the transmission tube is small and positively correlated, indicating that the change in length has almost no effect on the stress. Design variables P1 and P2 have positive and negative sensitivities to P6. The design variable P1 has a greater effect on the deformation and is negatively correlated, indicating that the deformation of the transmission tube decreases with the increase in the value of P1. The sensitivity of P2 to the transmission tube is positive, indicating that the deformation increases with the increase in P2.

In summary, P1 has the most significant effect on the maximum equivalent stress, and P2 has the most significant effect on the mass.

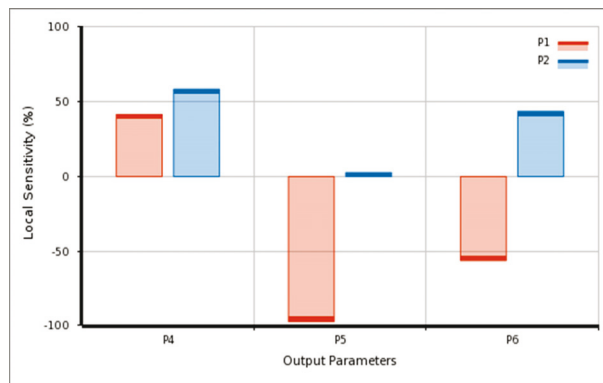


Fig. 14 Sensitivity of design variables P1 and P2 to the mass, maximum equivalent stress, and maximum deformation of the transmission tube

4.2.3 Selection of the optimization algorithm

According to the optimized design mathematical model (Equation 1), the objective of this optimized design is to set the minimum stress of the transmission tube and the mass $\leq 12,540$ kg. After the optimization objective is set, the multi-objective genetic algorithm is selected in the optimization method to solve the mathematical model for calculation. Approximately 100 groups of initial sample points are set, and each group of samples is repeated up to 70 times. After completing 596 convergence evaluations, three sets of optimal design points are obtained, as shown in Table 3.

Table 3 Three groups of optimal design points after transmission tube optimization

Parameters	Group 1	Group 2	Group 3
P1 (mm)	74.717	73.892	73.873
P2 (mm)	3117.1	3163.9	3183.8
P4 (kg)	12278	12332	12394
P5 (MPa)	55.57	56.42	56.45
P6 (mm)	0.776	0.794	0.797

Thereafter, the analysis of the three groups of optimal design points derived from Table 3 and their comparison are performed. Taking the first group of parameters as the standard, the rounded values are taken as the actual size of this transmission tube optimization, as shown in Table 4.

Table 4 Comparison of the dimensional parameters of the transmission tube before and after optimization

Parameters	Initial value before optimization	Initial value after optimization	Rounded values
P1 (mm)	70	74.717	75
P2 (mm)	3600	3117.1	3117

In Table 4, the value of P1 greatly increases, while that of P2 significantly decreases after optimization. The maximum equivalent stress of the optimized transmission tube is reduced from 60.84 MPa to 55.57 MPa, which is a reduction of approximately 8.662%. Meanwhile, the mass is reduced from 13,200 kg to 12,278 kg, which is a reduction of 6.985%.

4.3 Comparative analysis of stress and deformation before and after optimization

The original transmission tube model is modified in size based on the rounded values in Table 4. After the modification is completed, a static analysis is performed to verify the accuracy of the response surface method optimization. The same boundary conditions are set before and after the optimization of the simplified model of the transmission tube to ensure the reliability of the comparative analysis (Fig. 10).

4.3.1 Comparison of the transmission tube strength before and after optimization

The maximum equivalent stress values before and after the transmission tube optimization are shown in Fig. 15. The analysis shows that the maximum equivalent stress values before and after the optimization occur at the transition rounding on the discharge port. The maximum equivalent stress before optimization is 60.84 MPa, and that after optimization is 55.25 MPa, with a reduction of 9.19%. This indicates that the stress on the transmission tube has been significantly reduced after optimization.

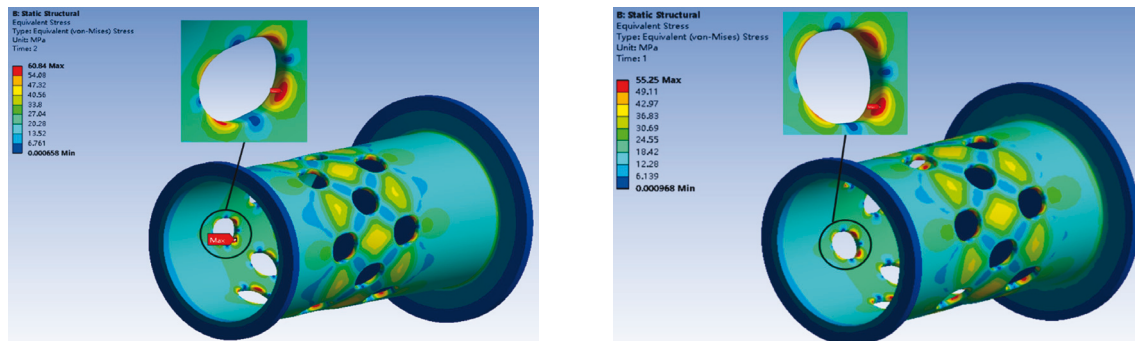


Fig. 15 Comparison of the maximum equivalent stress before and after the transmission tube optimization

4.3.2 Comparison of deformation before and after the transmission tube optimization

Figure 16 shows the deformation before and after the transmission tube optimization. The analysis shows that the maximum deformation before and after the transmission tube optimization occurs at their right ends. The maximum deformation before optimization is 0.927 mm, and that after optimization is 0.772 mm. The deformation of the transmission tube has been significantly reduced after the optimization.

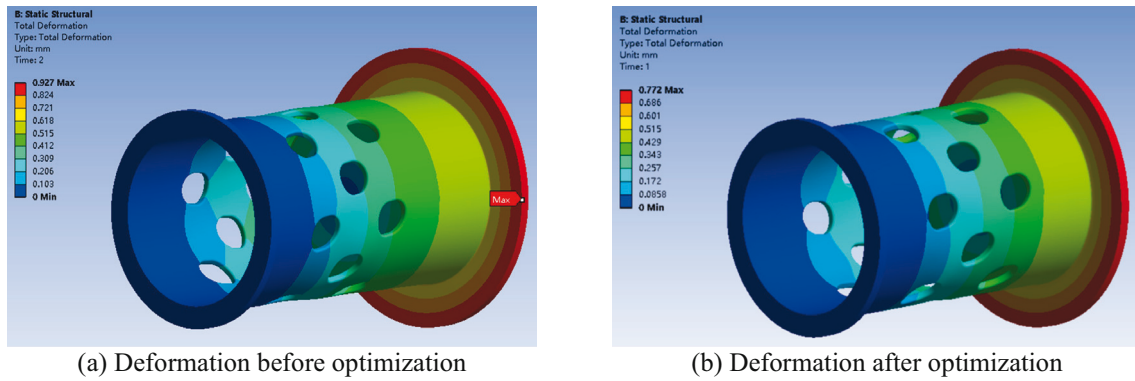


Fig. 16 Comparison of the deformation of the transmission tube before and after the optimization

Structural optimization of the dimensions of the transmission tube is carried out based on the response surface method and multi-objective genetic algorithm. A better optimization effect was achieved, as shown by the optimization results in Table 5. The optimized design reduces the mass of the transmission tube by 6.735% (from 13,200 kg to 12,311 kg), the maximum equivalent force by 9.188% (from 60.84 MPa to 55.25 MPa), and the maximum deformation by 16.721% (from 0.927 mm to 0.772 mm). These results show that the optimized method can effectively improve the performance and reliability of the transmission tube to meet the requirements of practical applications.

Table 5 Comparison of the response surface method optimization results

Parameters	Initial value before optimization	Initial value after optimization	Actual value after optimization	Range of variations
P4 (kg)	13,200	12,278	12,311	-6.735%
P5 (MPa)	60.84	55.57	55.25	-9.188%
P6 (mm)	0.927	0.776	0.772	-16.721%

5. Conclusion

The response surface method is used to optimize the structure of the ball mill transmission tube to resolve the problems of large size and low material utilization. The optimization is aimed at improving the performance and economic benefits of the ball mill and provides a more optimized reference solution for practical engineering applications. The main findings and conclusions of this paper are:

(1) The motion of the material in the transmission tube is analysed by EDEM. The result shows that at the moment when the materials fall into the transmission tube, they exert a large impact on the inner surface of the transmission tube and cause wear. After a certain period of operation, the transmission tube discharge port will wear more than its inner surface. Although there is some wear on the transmission tube, the overall depth of wear is small and will not affect the operational safety of the ball mill.

(2) The static analysis of the transmission tube using the EDEM-Workbench method shows that the maximum deformation of the transmission tube under the full load is 0.927 mm. The maximum equivalent stress is 60.84 MPa, which is much less than the permissible strength limit of the material (235 MPa). This indicates clearly that there is a significant improvement in the optimized design of the structure.

(3) Structural optimization of the transmission tube is based on the response surface method and multi-objective genetic algorithm. The results show that the maximum equivalent stress, mass, and maximum deformation of the optimized transmission tube are reduced by

9.188%, 6.735%, and 16.721%, respectively. After optimization, the mass of the transmission tube is significantly reduced, and the mechanical properties are also improved considerably, which achieves the optimization goal. These results not only provide firm theoretical support for the related research but also establish a solid foundation for further exploration and practical application.

Acknowledgements

This research was financially supported by the Jiangsu ‘Six Talent Peak’ Project (JXQC-022).

Declaration of competing interest

The authors declare that they have no known competing financial interests or personal relationships that could have appeared to influence the work reported in this paper.

REFERENCES

- [1] Fragoso A, Martins RF, Soares AC. Failure analysis of a ball mill located in a cement’s production line. *Engineering Failure Analysis* 2022;138. <https://doi.org/10.1016/j.engfailanal.2022.106339>
- [2] Nagesha KV, Arunkumar D, Kumar GM, Yadav R, Khakha U, Vishwakarma B, et al. Parametric study on four station ball mill for synthesis of ultrafine powders. *Materials Today: Proceedings* 2023. <https://doi.org/10.1016/j.matpr.2023.04.360>
- [3] Santosh T, Eswaraiiah C, Soni RK, Kumar S. Size reduction performance evaluation of HPGR/ball mill and HPGR/stirred mill for PGE bearing chromite ore. *Advanced Powder Technology* 2023;34. <https://doi.org/10.1016/j.appt.2022.103907>
- [4] Pareek P, Sankhla VS. Review on vertical roller mill in cement industry & its performance parameters. *Materials Today: Proceedings* 2021;44:4621–7. <https://doi.org/10.1016/j.matpr.2020.10.916>
- [5] Xie C, Zhao Y. Investigation of the ball wear in a planetary mill by DEM simulation. *Powder Technology* 2022;398. <https://doi.org/10.1016/j.powtec.2021.117057>
- [6] Carvalho RM de, Campos TM, Faria PM, Tavares LM. Mechanistic modeling and simulation of grinding iron ore pellet feed in pilot and industrial-scale ball mills. *Powder Technology* 2021;392:489–502. <https://doi.org/10.1016/j.powtec.2021.07.030>
- [7] Hanumanthappa H, Vardhan H, Mandela GR, Kaza M, Sah R, Shanmugam BK. A comparative study on a newly designed ball mill and the conventional ball mill performance with respect to the particle size distribution and recirculating load at the discharge end. *Minerals Engineering* 2020;145. <https://doi.org/10.1016/j.mineng.2019.106091>
- [8] Bilgili E, Guner G. Mechanistic Modeling of Wet Stirred Media Milling for Production of Drug Nanosuspensions. *AAPS PHARMSCITECH* 2021;22. <https://doi.org/10.1208/s12249-020-01876-w>
- [9] Zhang Z, Ma C, Sun J, Zhang Y, Ni X. A Method for Calculating the Reliability of Welded Metal Bellows for Mechanical Seals. *Coatings* 2022;12. <https://doi.org/10.3390/coatings12020175>
- [10] Krizhanovsky VV, Mali VI, Prueel ER. Discrete Element Study of Granule Consolidation. *Physical Mesomechanics* 2022;25:149–54. <https://doi.org/10.1134/S1029959922020060>
- [11] Bannoud MA, Martins TD, Santos BF dos. Control of a closed dry grinding circuit with ball mills using predictive control based on neural networks. *Digital Chemical Engineering* 2022;5. <https://doi.org/10.1016/j.dche.2022.100064>
- [12] Fragniere G, Naumann A, Schrader M, Kwade A, Schilde C. Grinding Media Motion and Collisions in Different Zones of Stirred Media Mills. *MINERALS* 2021;11. <https://doi.org/10.3390/min11020185>
- [13] Osborne T, Rhymer D, Werner D, Ingram A, Windows-Yule CRK. Investigating the impact of impeller geometry for a stirred mill using the discrete element method: Effect of pin number and thickness. *POWDER TECHNOLOGY* 2023;428. <https://doi.org/10.1016/j.powtec.2023.118810>
- [14] Chimwani N, Bwalya MM. Using DEM to investigate how shell liner can induce ball segregation in a ball mill. *Minerals Engineering* 2020;151. <https://doi.org/10.1016/j.mineng.2020.106311>
- [15] Zhou S, Wang Q, Liu J. Control Strategy and Simulation of the Regenerative Braking of an Electric Vehicle Based on an Electromechanical Brake. *Transactions of FAMENA* 2022

- [16] Zhang Y, Li L. Introduction and implementation of fluid forces in a DEM code for simulating particle settlement in fluids. *Powder Technology* 2024;433. <https://doi.org/10.1016/j.powtec.2023.119238>
- [17] Kim K-C, Jiang T, Kim N-I, Kwon C. Effects of ball-to-powder diameter ratio and powder particle shape on EDEM simulation in a planetary ball mill. *Journal of the Indian Chemical Society* 2022;99:100300. <https://doi.org/10.1016/j.jics.2021.100300>
- [18] Wang Y, Wang G, Wu S, Liu Z, Fang Y. A calibration method for ore bonded particle model based on deep learning neural network. *Powder Technology* 2023;420. <https://doi.org/10.1016/j.powtec.2023.118417>
- [19] Liu C, Lin W. Numerical and Experimental Analysis of Roller Hemming on Door Panel's Curved and Straight-Edge of Flat Plane. *Applied Sciences* 2024;14. <https://doi.org/10.3390/app142110066>
- [20] Bor A, Jargalsaikhan B, Uranchimeg K, Lee J, Choi H. Particle morphology control of metal powder with various experimental conditions using ball milling. *Powder Technology* 2021;394:181–90. <https://doi.org/10.1016/j.powtec.2021.08.053>
- [21] Ni C, Wang D, Vinson R, Holmes M, Tao Y. Automatic inspection machine for maize kernels based on deep convolutional neural networks. *Biosystems Engineering* 2019;178:131–44. <https://doi.org/10.1016/j.biosystemseng.2018.11.010>
- [22] Aghababaei R, Zhao K. Micromechanics of material detachment during adhesive wear: A numerical assessment of Archard's wear model. *Wear* 2021;476. <https://doi.org/10.1016/j.wear.2021.203739>
- [23] Sun Y, Li Y, Zhang Q, Qin X, Chen K. Wear analysis and simulation of small module gear based on Archard model. *Engineering Failure Analysis* 2023;144. <https://doi.org/10.1016/j.engfailanal.2022.106990>
- [24] Ghalandari V, Iranmanesh A. Energy and exergy analyses for a cement ball mill of a new generation cement plant and optimizing grinding process: A case study. *Advanced Powder Technology* 2020;31:1796–810. <https://doi.org/10.1016/j.appt.2020.02.013>
- [25] Fragoso A, Martins RF, Soares AC. Failure analysis of a ball mill located in a cement's production line. *Engineering Failure Analysis* 2022;138. <https://doi.org/10.1016/j.engfailanal.2022.106339>
- [26] Kou Q, Bu L, Chen J, Sugirbay A. Design of an Air-Assisted Mechanical Seed-Metering Device for Millet (*Setaria Italica*) Based on Experiments and Simulation Analysis. *Tehnički Vjesnik - Technical Gazette* 2024;31:628–36. <https://doi.org/10.17559/TV-20230117000231>
- [27] Wang G, Zhao H, Liang H, Deng C, Ma W. Multi-objective optimisation of process parameters for laser-based directed energy deposition of a mixture of H13 and M2 steel powders on 4Cr5Mo2SiV1 steel. *Virtual and Physical Prototyping* 2024;19. <https://doi.org/10.1080/17452759.2023.2290184>
- [28] Golubić L, Gršić J, Bušić M, Tomić T. Application of Response Surface Methodology in the Analysis of Weldability Test Results on X80 Steel. *Tehnički Glasnik* 2023;17:486–92. <https://doi.org/10.31803/tg-20220720154258>
- [29] Pang Q, Xiong J. Prediction Model of Three-Dimensional Machined Potassium Dihydrogen Phosphate Surfaces Based on a Dynamic Response Machining System. *Materials* 2022;15. <https://doi.org/10.3390/ma15249068>
- [30] Li G, Wu C, Xu K, Ran Q, Cao B. Pivotal errors identification of the face gear worm grinding machine tool with a piecewise sensitivity analysis. *Mechanism and Machine Theory* 2023;181. <https://doi.org/10.1016/j.mechmachtheory.2022.105206>

Submitted: 14.6.2024

Accepted: 20.12.2024

You Zhou
Jicheng Shen
Weihua Wei*
College of Mechanical and Engineering,
Nanjing Forestry University, Nanjing, China
Fang Luo
Jiangsu Jinxiang Transmission Equipment
Co. Ltd., Huaian, China
*Corresponding author:
whwei@njfu.edu.cn